J of Nuclear Medicine Technology, first published online April 19, 2022 as doi:10.2967/jnmt.121.263240

Continuous bed motion in a silicon photomultiplier-based scanner provides equivalent spatial resolution and image quality in whole body PET images at similar acquisition times using the step-and-shoot method

Kodai Kumamoto[1], Hideaki Sato[1], Yuji Tsutsui[2], Shinichi Awamoto[3], Yasuo Yamashita[3], Shingo Baba[4], Masayuki Sasaki[5]

[1]Department of Health Sciences, Graduate School of Medical Sciences, Kyushu University, Fukuoka, Japan

[2]Department of Radiological Science, Faculty of Health Science, Junshin Gakuen University

[3]Division of Radiological Technology, Department of Medical Technology, Kyushu University Hospital

[4]Department of Clinical Radiology, Graduate School of Medical Sciences, Kyushu University

[5]Department of Health Sciences, Faculty of Medical Sciences, Kyushu University

short running title

Continuous bed motion in SiPM-PET

Corresponding author

Masayuki Sasaki, MD, PhD

Department of Medical Quantum Science, Faculty of Medical Sciences, Kyushu University

3-1-1 Maidashi, Higashi-ku, Fukuoka 812-8582, Japan

TEL: +81-92-642-6746, FAX: +81-92-642-6723

E-mail: sasaki.masayuki.165@m.kyushu-u.ac.jp

First author

Kodai Kumamoto

Department of Medical Quantum Science, Graduate School of Medical Sciences, Kyushu University

3-1-1 Maidashi, Higashi-ku, Fukuoka 812-8582, Japan

TEL: +81-92-642-6746, FAX: +81-92-642-6723

E-mail: kumamoto.kodai.313@s.kyushu-u.ac.jp

(manuscript: 2651 words)

Abstract

This study investigated the spatial resolution and image quality of the continuous bed motion (CBM) method in a sensitive silicon photomultiplier (SiPM)-based positron emission tomography (PET)/computed tomography (CT) system compared with the traditional step-and-shoot (SS) method.

Methods: Siemens Biograph Vision was used in this study. Data acquisition using the SS method was performed for 3 min per bed. In the CBM method, the bed speed ranged from 0.5 to 3.3 mm/s. The acquisition time equivalent to the SS method was 1.1 mm/s for 2-bed ranges and 0.8 mm/s for seven-bed ranges. The spatial resolution was investigated using ^{18}F point sources and evaluated using the full width at half maximum. Image quality was investigated using a National Electrical Manufacturers Association International Electrotechnical Commission body phantom with six spheres 10-, 13-, 17-, 22-, 28-, and 37-mm inner diameters. The radioactivity concentration ratio of the ^{18}F solution in all spheres and the background was approximately 4:1. The detectability of each sphere was visually evaluated on a five-step score. Image quality was physically evaluated using the noise equivalent count rate ($NEC_{phantom}$), contrast percentage of the 10-mm hot sphere ($Q_{H,10mm}$), background variability percentage (N_{10mm}), and contrast–noise ratio ($Q_{H,10mm}/N_{10mm}$).

Results: The spatial resolution was not affected by the difference of acquisition methods and bed speeds. The detectability of the 10-mm sphere with a bed speed of 2.2 mm/s or faster was significantly inferior to

that of the SS 2-bed method. In evaluating image quality, no significant difference in the contrast percentage was observed among the acquisition methods and speeds in the CBM method. However, the increasing bed speed in the CBM method increased the N_{10mm} and decreased the $NEC_{phantom}$. When comparing the SS 2-bed method with the CBM method at 0.8 mm/s, no significant differences in all parameters were observed.

Conclusions: In a SiPM-based PET/CT scanner, the CBM method provides equivalent spatial resolution and image quality in whole body PET images with same acquisition time using the SS method.

(325 words)

Key words: continuous bed motion; step-and-shoot; SiPM; spatial resolution; image quality

INTRODUCTION

The step-and-shoot (SS) method has been traditionally used for positron emission tomography (PET) data acquisition; however, the continuous bed motion (CBM) method has recently been developed. In the SS method, multi-bed data are sequentially acquired only when the bed is stationary, but are not acquired when the bed is moving (*1-10*). Longer than 1 min is wasted in a whole-body acquisition. Moreover, the axial acquisition range is determined by the number of beds, resulting in an unnecessary acquisition range and radiation exposure in computed tomography (CT) scan. In the CBM method, the bed continuously moves to acquire data (*2-10*), the axial acquisition range can be determined in a 0.1-mm unit, and the bed speed can be changed according to the body part (*2,3,6,8,9*). Moreover, generating a whole-body image by adding several fast whole-body scans should be useful in case of interruptions in the examination due to patient motion or pain (*7,11*). It has been reported that patients preferred continuous bed movements more than SS movements (*6*). Therefore, the CBM method may replace the SS method because of the flexible PET examination for each patient. The usefulness of the CBM method in PET/CT using the photomultiplier tube (PMT) system has been studied (*2-11*). The differences between the SS and CBM methods did not significantly affect the maximum or mean standardized uptake values in phantoms or tumors in clinical examinations (*3,4,6-9*). In contrast, the SS method has been reported to be superior to the CBM method in terms of variability in the background region (*4,9*).

Silicon photomultiplier (SiPM), which is a semiconductor detector, was recently applied in PET/CT scanners instead of the traditional PMT (*12-14*). Compared with conventional PMT-based PET scanners, SiPM-based PET scanners achieved a high gain and faster time response. This feature improves the sensitivity and time-of-flight (TOF) timing resolution, thus resulting in a good image quality, short examination time, and decrease in administration dose and radiation exposure (*15-17*). With these advantages, the CBM method using SiPM-based PET/CT scanners is expected to provide same sufficient image quality with flexible examinations. However, the usefulness of the CBM method in SiPM-based PET/CT scanners has not been studied.

In this study, we investigated the image quality of the CBM method in SiPM-based PET/CT systems compared with the conventional SS method. Moreover, we evaluated the influence of varying bed speeds on image quality.

MATERIALS AND METHODS

PET/CT scanner

PET data were acquired using the Biograph Vision PET/CT scanner (Siemens Healthineers, Knoxville, USA). The PET system has eight rings based on 38 detector blocks with lutetium oxyorthosilicate

(Lu_2SiO_5:Ce) crystals (3.2 × 3.2 × 20 mm) with 6,400 crystals per ring. The transverse field of view (FOV) was 700 mm, and the axial FOV was 263 mm. The spatial resolution at 1 cm with full width at half maximum (FWHM) was 3.7 mm. The TOF timing resolution was 214 psec, and the coincidence time window was 4.7 nsec. These values are reported by the manufacturer. The CT system has 64 rows, and the rotation time was 0.33 sec. CT images can be obtained using the following parameters: 70–120 kV, 20–666 mA, 0.5-s tube rotation, 0.8 pitch, and a 0.6-mm slice collimation. In this study, the voltage was 120 kVp and the tube current was set by CT automatic exposure control.

Point source phantom

The spatial resolution was investigated using ^{18}F point sources. One μL of ^{18}F solution was put in glass capillaries with an inner diameter of 0.70 mm and an outer diameter of 0.97 mm. The radioactivity concentration was 30 MBq/mL. Point sources were placed at transaxial positions (1, 0), (10, 0), and (0, 10) cm on the same z-position.

Body phantom

Image quality was investigated using a National Electrical Manufacturers Association (NEMA) International Electrotechnical Commission body phantom (Data Spectrum Corp., Durham, NC, USA) with six spheres of 10-, 13-, 17-, 22-, 28-, and 37-mm inner diameters. The body phantom was an acrylic phantom that mimicked the torso of a human weighing 60 kg. The body phantom had a long diameter of

300 mm, a short diameter of 230 mm, a circumference of 840 mm, a height of 180 mm, and a volume of 9.7 L (Supplemental Fig. 1). The radioactivity concentration of ^{18}F solution in all spheres and the background were approximately 10.6 and 2.65 kBq/mL (ratio of 4:1), respectively. The radioactivity concentration was measured using an automatic well gamma counter (AccuFLEX γ7001, Hitachi Aloka Medical, Ltd., Japan).

Data acquisition and image reconstruction

In the SS method, data acquisition was performed for 3 min/bed x 1 bed and 3 min/bed x 2 beds in the list mode according to the paper reported by Tsutsui et al (*15*). The 1-bed acquisition was for the standard acquisition, while the 2-bed acquisition for the overlapping acquisition. The overlap in multi-bed acquisition was 49.8%, as determined by the manufacturer to improve the sensitivity distribution in the z-axis. In the CBM method, the bed speeds of 0.5, 0.8, 1.1, 2.2, and 3.3 mm/s were investigated. Whole body acquisition from the top of the head to the mid-thigh usually requires 7 or 8 bed positions in the standard SS method among Japanese institutions. The regional acquisition time of 0.8 mm/s in the CBM method was consistent with that of 8-bed acquisition with 3 min/bed in the SS method. The 1.1 mm/s bed speed was consistent with 2-bed acquisition with 3 min/bed in the SS method.

In the spatial resolution investigation, PET images were reconstructed using filtered back projection. The image matrix was 440 × 440 (1.65 × 1.65 mm), and the slice thicknesses were 1.65, 3.00,

and 5.00 mm. Attenuation and scattering corrections were not used. In the image quality investigation, PET images were reconstructed using ordered-subsets expectation maximization with point-spread-function correction and TOF information. This study used 3 iterations and 5 subsets for the NEMA IQ. Three iterations were done in accordance with our previous report (*15*). The Biograph Vision scanners employ 5 subsets by default; this is fixed by the manufacturer and is unchangeable. CT attenuation correction was performed. Scatter corrections were performed using single-scatter simulation. A Gaussian filter was not used. The image matrix was 440 × 440, and the slice thickness was 1.65 mm.

Measurement of spatial resolution

The spatial resolution was evaluated using the FWHM. Profile curves of each point source in the x-, y-, and z-directions were created passing through the highest count pixel on the highest count slice using ImageJ (National Institutes of Health Image, USA). In the profile curve, the maximum count was determined using a parabolic approximation using one point with the highest pixel count and two adjacent points. The FWHM of the three directions in each position was calculated by linearly interpolating between adjacent pixels at half the maximum value of the response function. FWHM $x_{(a, b)}$ is FWHM in the x-direction at position (a,b). The spatial resolution was evaluated using the FWHM of 1 cm transverse, 10 cm transverse radial, and 10 cm transverse tangential and axial directions. These were calculated using the following equations:

・$FWHM_{1\ cm}$ $= \{FWHM\ x_{(0,\ 1)} + FWHM\ y_{(0,\ 1)}\} /2$

・$FWHM_{10\ cm\ radial}$ $= \{FWHM\ x_{(10,\ 0)} + FWHM\ y_{(0,\ 10)}\} / 2$

・$FWHM_{10\ cm\ tangential}$ $= \{FWHM\ y_{(10,\ 0)} + FWHM\ x_{(0,\ 10)}\} / 2$

・$FWHM_{axial}$ $= \{FWHM\ z_{(0,\ 1)} + FWHM\ z_{(0,\ 10)} + FWHM_{z\ (10,\ 0)}\} / 3$

Assessment of image quality

The detectability of each sphere was visually evaluated on a five-step score (1, not absolutely visualized; 2, may not be visualized; 3, uncertain; 4, maybe visualized; and 5, absolutely visualized) by a board-certified nuclear medicine physician and two radiological technologists. Scores were averaged for each sphere. Fukukita et al. reported that they decided to use the score of the 10-mm sphere as the reference value because image quality and spatial resolution are most affected by the ability to visualize the 10-mm sphere (*18*). Therefore, we mainly evaluated the visual scores of the 10-mm sphere. The inter-observer agreement was evaluated using the kappa coefficient.

In the NEMA body phantom PET images, the slice in which the hot sphere was most clearly observed was designated as the center slice. A region of interest (ROI) on the 10-mm hot sphere was placed in the center slice with the same size of the inner diameter. Twelve circular ROIs with diameters of 10 mm and 37 mm were placed in the background on the center slice at ±1 cm and ±2 cm from the center slice (60 ROIs in total). According to the phantom test procedure for whole-body PET imaging with ^{18}F-FDG

(*18*), the noise equivalent counts ($NEC_{phantom}$), contrast percentage of the 10-mm hot sphere ($Q_{H,\ 10mm}$), background variability percentage (N_{10mm}), and contrast–noise ratio (Q_{10mm}/N_{10mm}) were calculated using the following equations. True, scatter, and random coincidences were acquired from a sinogram header, and scatter fraction (SF) and random scaling factor were acquired from a default value. These processes were performed using the PMOD software (version 3.8; PMOD Technologies LLC., Zürich, Switzerland).

$$\cdot\ NEC_{phantom} = (1-SF)^2 \frac{(T+S)^2}{(T+S)+(1+k)fR}\ (Mcounts)$$

$$f = \frac{S_a}{\pi r^2}$$

where T, S, and R correspond to true, scatter, and random coincidences acquired within the scanning period, respectively. Moreover, SF and k are the scatter fraction and random scaling factor, respectively. The SF of Biograph Vision scanners is fixed at 0.39 by the manufacturer. The k is set to 0 because we used variance reduction techniques for estimating a smooth random distribution (*18*). The f is the ratio of object size to FOV. S_a is the cross-sectional area of the phantom. Finally, r is the radius of the detector ring diameter.

$$\cdot\ Q_{H,10mm} = \frac{C_{H,10mm}/C_{B,10mm} - 1}{a_H/a_B - 1} \times 100\ (\%)$$

where $C_{H,\ 10mm}$ is the average count in the ROI for a 10-mm sphere. $C_{B,\ 10mm}$ is the average count of the 60 background ROIs of 10-mm diameter. Finally, a_H and a_B are the radioactivity concentrations in the hot sphere and background, respectively.

・$N_{10mm} = \frac{SD_{10mm}}{C_{B,10mm}} \times 100\ (\%)$

$SD_{10mm} = \sqrt{\sum_{k=1}^{K}(C_{B,10mm,k} - C_{B,10mm})^2/(K-1)}$, K=60,

where SD_{10mm} is the standard deviation of the background ROIs of 10-mm diameter.

・Q_{10mm}/N_{10mm}

Statistical analysis

JMP Pro 15 (SAS Institute Inc., Cary, NC, USA) was used for statistical analysis. The Tukey test was employed to analyze the significance of the differences between the SS 2-bed method and the CBM method in each bed speed. *P*-values of less than 0.05 were used to denote statistical significance.

RESULTS

Comparison of the spatial resolution

Figure 1 shows the PET images of point sources at position (0,1) cm. In the axial images, the shape and size were not different among the acquisition methods or bed speeds. In the coronal images, the image extended in the body axis direction in association with an increase in the slice thickness. However, no differences in shape and size were visually observed among the different bed speeds.

Figure 2 shows the FWHM of the x- and y-directions. No significant differences in the $FWHM_{1\ cm}$, $FWHM_{10\ cm\ radial}$, and $FWHM_{10\ cm\ tangential}$ were observed between the SS and CBM methods. Moreover, the difference in the FWHM results when varying the slice thickness was insignificant. Figure 3 shows the $FWHM_{axial}$. As the slice thickness increased, the $FWHM_{axial}$ significantly increased. However, no significant difference in the $FWHM_{axial}$ was observed between the SS and CBM methods and among the various bed speeds in the CBM method.

Assessment of image quality

Figure 4 shows the PET images of the NEMA body phantom in the SS and CBM methods. In the SS method, the clarity of the hot spheres and background variability were not visually different between 1-bed and 2-bed acquisitions. In the CBM method, the background variability increased as the bed speed increased. Figure 5 shows the results of the visual evaluation. The detectability of the 10-mm sphere with bed speeds faster than 2.2 mm/s was significantly inferior to that with the SS 2-bed method ($P < 0.05$). In the SS method, the score of the 10-mm sphere was above 4. In the CBM method, the bed speed should be 1.1 mm/s or slower to exceed the 10-mm sphere score of 3. The inter-observer agreement was moderate ($\kappa = 0.55$).

Figure 6 shows the comparison of the $NEC_{phantom}$. In the CBM method, the $NEC_{phantom}$ decreased as the bed speed increased. The $NEC_{phantom}$ in the CBM method with bed speeds of 1.1 mm/s or faster were

significantly inferior than that in the SS 2-bed method ($P < 0.05$). Figure 7 shows the results of the physical assessment of image quality. No significant difference in $Q_{H,10mm}$ was observed between the SS and CBM methods and among the various bed speeds in the CBM method (Fig. 7A). Figure 7B shows the comparison of N_{10mm}. In the SS method, no difference in the N_{10mm} was observed between 1-bed and 2-bed acquisitions. In the CBM method, the N_{10mm} increased as the bed speed increased. The N_{10mm} in the CBM method with bed speeds of 1.1 mm/s or faster were significantly inferior than that in the SS 2-bed method ($P < 0.05$). Figure 7C shows the comparison of the Q_{10mm}/N_{10mm}. The Q_{10mm}/N_{10mm} was not different within the SS method, whereas, in the CBM method, it decreased as the bed speed increased. The Q_{10mm}/N_{10mm} in the CBM method with bed speeds of 2.2 mm/s or faster was significantly lower than that in the SS 2-bed method ($P < 0.05$).

DISCUSSION

Using the SiPM-based PET/CT scanner, the spatial resolution was not significantly different between the SS and CBM methods and among the different bed speeds in the CBM method even when the slice thickness was changed. The $NEC_{phantom}$ decreased as the bed speed increased in the CBM method. In assessing image quality, the background variability significantly increased as the bed speeds increased. However, the contrast of the hot sphere showed no difference among the acquisition methods and bed speeds.

The spatial resolution was not significantly different between the SS and CBM methods and among the bed speeds in CBM method. In the coronal planes, the FWHM increased as the slice thickness increased, but no significant difference was observed between the acquisition methods and among the different bed speeds. Because the PET data was acquired during continuous movement in the CBM method, image blurring was considered to increase the body axial FWHM. Furthermore, the increase of bed speed was also considered to exacerbate the spatial resolution. In the CBM method, when the bed was shifted by a distance equal to the separation between sinogram planes, the events from the same detector were assigned to the next image plane. In the scanner used in this study, the CBM method data were separated and organized by the same axial sampling of 1.65 mm as in the SS method (*5*). Objects smaller than the pixel size were distributed uniformly over the entire pixel, rather than at the center of the pixel. Thus, no significant difference was observed when the bed speed was changed by this function. In the transverse slice, the FWHM did not change when the slice thickness was increased because the pixel sizes were all the same.

The $NEC_{phantom}$ using the NEMA body phantom showed no significant difference between the SS 2-bed acquisition and 0.8 mm/s of the CBM method. The $NEC_{phantom}$ decreased as the bed speed increased. Because the acquisition time decreased as the bed speed increased, the $NEC_{phantom}$ decreased due to reduced coincidence counts. This result is consistent with that reported in a previous study (*7,15*).

The background variability also increased as the bed speed increased. The increase in the variability with decreasing counts is consistent with that reported in a previous study (*15,19*). Regarding the background variability, the SS method on the PMT-based scanner was significantly superior to the CBM method using the same acquisition time (*4,9*). In contrast, that of the SS method was comparable to that of the CBM method on the SiPM-based scanner in this study. The improvement of the scanner's sensitivity and extension of the axial FOV in the SiPM system in this study is considered to improve the image quality of the CBM method. The visibility of the 10-mm hot sphere is not different between the SS 2-bed acquisition and 0.8 mm/s of the CBM method, and the visual score decreased as the bed speed increased. This is probably due to the increase in noise caused by the decrease in coincidence counts (*20*). The contrast values remained the same at all bed speeds. This tendency has also been shown in a past study (*9,15*).

This study has some limitations. First, the number of varieties of bed speeds examined was limited. An examination with further varieties of bed speeds might discover the appropriate bed speed equivalent to the SS method. Second, the CBM method was performed in one way only. The image quality of the summed to-and-fro pass images should be examined. Third, the axial sampling size examined was fixed at 1.65 mm. A smaller axial sampling size may improve the axial spatial resolution. Lastly, further clinical examination should be conducted to compare the SS and CBM methods.

CONCLUSION

Our findings show that for SiPM-based PET/CT systems, image quality metric results were comparable between the SS method for 3 min/bed and the CBM method for speeds of 0.8 mm/s at almost the same acquisition time in whole body acquisitions. It is expected that the CBM method is chosen in some cases depending on the combination of bed speeds.

DISCLOSURE

The authors have no potential conflicts of interest relevant to this article to declare.

ACKNOWLEDGMENTS

We thank Kyushu University Hospital and its nuclear medicine and PET center team for allowing the use of their equipment and radioactive material.

KEY POINTS

QUESTION: Can the continuous bed motion method preserve spatial resolution and image quality of the traditional step-and-shoot method in a SiPM-PET/CT scanner?

PERTINENT FINDINGS: No difference in spatial resolution and image quality was observed between the SS method and the CBM 0.8 mm/s method at similar acquisition times in whole body acquisition.

IMPLICATIONS FOR PATIENT CARE: Since the CBM method preserves the same image quality as the SS method and provides a more flexible examination, it is expected to be widely used when whole-body acquisition is performed with semiconductor PET/CT systems in the future.

REFERENCES

1. Dahlbom M, Hoffman EJ, Hoh CK, et al. Whole-body positron emission tomography: Part I. Methods and performance characteristics. *J Nucl Med*. 1992;33:1191-9.

2. Acuff SN, Osborne D. Clinical Workflow Considerations for Implementation of Continuous-Bed-Motion PET/CT. *J Nucl Med Technol*. 2016;44:55-8.

3. Osborne DR, Acuff S, Cruise S, et al. Quantitative and qualitative comparison of continuous bed motion and traditional step and shoot PET/CT. *Am J Nucl Med Mol Imaging*. 2014 15;5:56-64.

4. Rausch I, Cal-González J, Dapra D, et al. Performance evaluation of the Biograph mCT Flow PET/CT system according to the NEMA NU2-2012 standard. *EJNMMI Phys*. 2015;2:26.

5. Panin VY, Smith AM, Hu J, Kehren F, Casey ME. Continuous bed motion on clinical scanner: design, data correction, and reconstruction. *Phys Med Biol*. 2014 21;59:6153-74.

6. Schatka I, Weiberg D, Reichelt S, et al. A randomized, double-blind, crossover comparison of novel continuous bed motion versus traditional bed position whole-body PET/CT imaging. *Eur J Nucl Med Mol Imaging*. 2016;43:711-7.

7. Yamamoto H, Takemoto S, Maebatake A, et al. Verification of image quality and quantification in whole-body positron emission tomography with continuous bed motion. *Ann Nucl med*. 2019;33:288-94

8. Meier JG, Erasmus JJ, Gladish GW, et al. Characterization of continuous bed motion effects on patient breathing and respiratory motion correction in PET/CT imaging. *J Appl Clin Med Phys*. 2020;21:158-165.

9. Yamashita S, Yamamoto H, Nakaichi T, Yoneyama T, Yokoyama K. Comparison of image quality between step-and-shoot and continuous bed motion techniques in whole-body ^{18}F-fluorodeoxyglucose positron emission tomography with the same acquisition duration. *Ann Nucl Med*. 2017;31:686-95.

10. Siman W, Kappadath SC. Comparison of Step-and-Shoot and Continuous-Bed-Motion PET Modes of Acquisition for Limited-View Organ Scans. *J Nucl Med Technol*. 2017;45:290-296.

11. Osborne DR, Acuff S. Whole-body dynamic imaging with continuous bed motion PET/CT. *Nucl Med Commun*. 2016;37:428-31.

12. Rausch I, Ruiz A, Valverde-Pascual I, Cal-González J, Beyer T, Carrio I. Performance evaluation of the Vereos PET/CT system according to the NEMA NU2-2012 standard. *J Nucl Med*. 2019;60:561-567.

13. Hsu DFC, Ilan E, Peterson WT, Uribe J, Lubberink M, Levin CS. Studies of a Next-Generation Silicon-Photomultiplier-Based Time-of-Flight PET/CT System. *J Nucl Med*. 2017;58:1511-1518.

14. van Sluis J, de Jong J, Schaar J, et al. Performance Characteristics of the Digital Biograph Vision

PET/CT System. *J Nucl Med*. 2019;60:1031-1036.

15. Tsutsui Y, Awamoto S, Himuro K, Kato T, Baba S, Sasaki M. Evaluating and comparing the image quality and quantification accuracy of SiPM-PET/CT and PMT-PET/CT. *Ann Nucl Med*. 2020;34:725-35

16. Wagatsuma K, Miwa K, Sakata M, et al. Comparison between new-generation SiPM-based and conventional PMT-based TOF-PET/CT. *Phys Med*. 2017;42:203-210.

17. Surti S, Viswanath V, Daube-Witherspoon ME, Conti M, Casey ME, Karp JS. Benefit of Improved Performance with State-of-the Art Digital PET/CT for Lesion Detection in Oncology. *J Nucl Med*. 2020;61:1684-1690.

18. Fukukita H, Suzuki K, Matsumoto K, et al. Japanese guideline for the oncology FDG-PET/CT data acquisition protocol: synopsis of version 2.0. *Ann Nucl Med*. 2014;28:693–705.

19. Hashimoto N, Morita K, Tsutsui Y, Himuro K, Baba S, Sasaki M. Time-of-Flight Information Improved the Detectability of Subcentimeter Spheres Using a Clinical PET/CT Scanner. *J Nucl Med Technol*. 2018;46:268-273.

20. Akamatsu G, Ikari Y, Nishida H, et al. Influence of Statistical Fluctuation on Reproducibility and Accuracy of SUVmax and SUVpeak: A Phantom Study. *J Nucl Med Technol*. 2015;43:222-6.

FIGURE 1. PET images of a point source at coordinates (0,1) cm. The upper figure shows axial images, and the lower one shows coronal images. No visual difference was observed among all acquisition methods, whereas the coronal images extended along with the increase in the slice thickness.

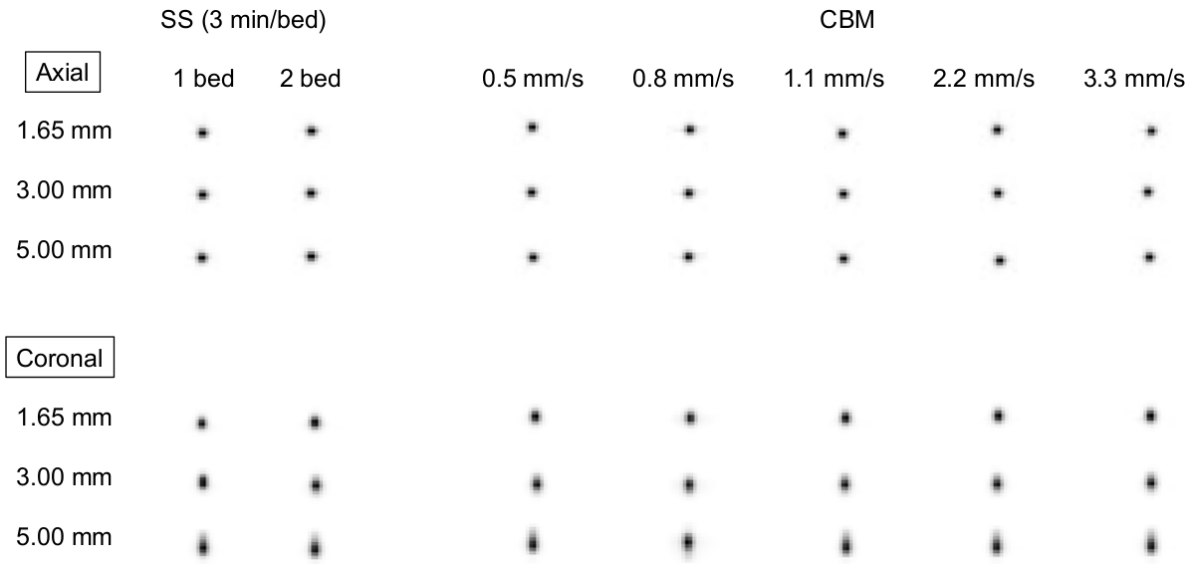

FIGURE 2. Comparison of the FWHM in axial plane of (A)1 cm, (B)10 cm radial, and (C)10 cm tangential. They were not significantly different between the SS and CBM methods and among different bed speeds in the CBM method even when the slice thickness was changed.

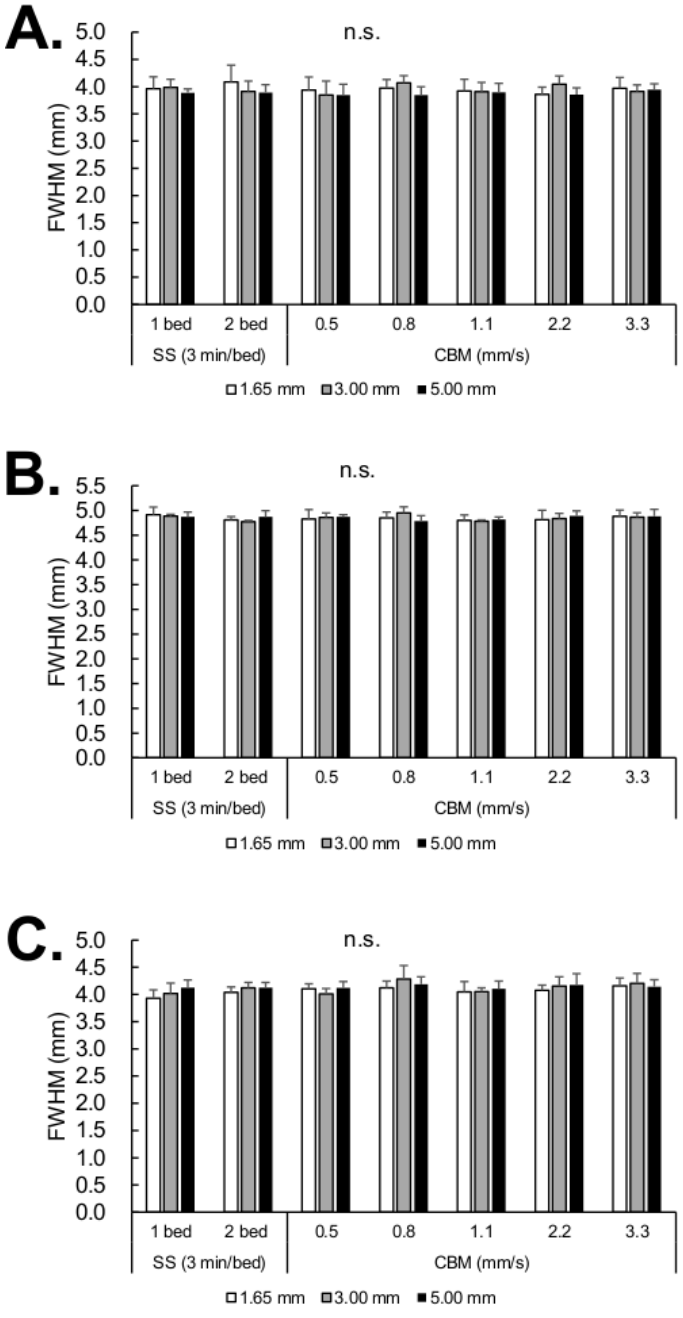

FIGURE 3. Comparison of the FWHM of the body axial direction. They were not significantly different among the different acquisition methods and bed speeds, whereas the FWHM significantly increased in thicker slices.

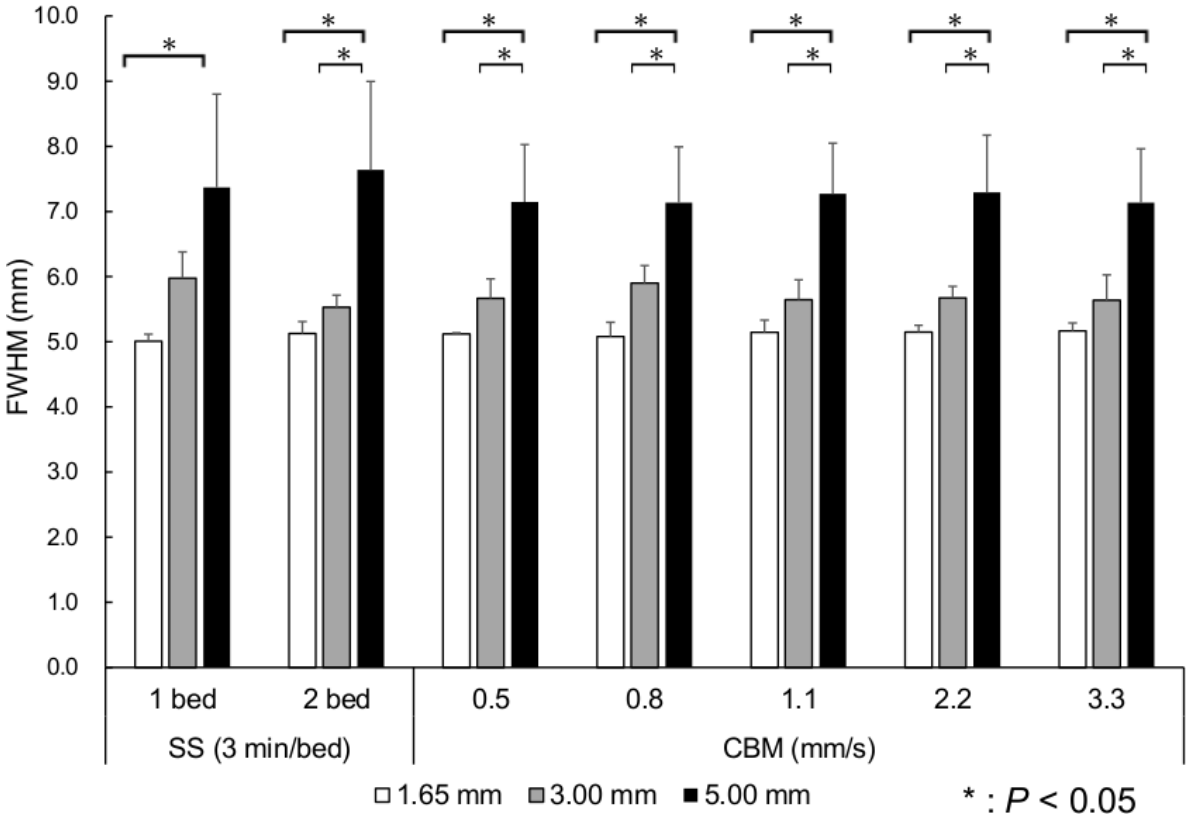

FIGURE 4. PET images of the body phantom using the SS method (top) and the CBM method (bottom). In the CBM method, images with faster bed speeds show high background variability.

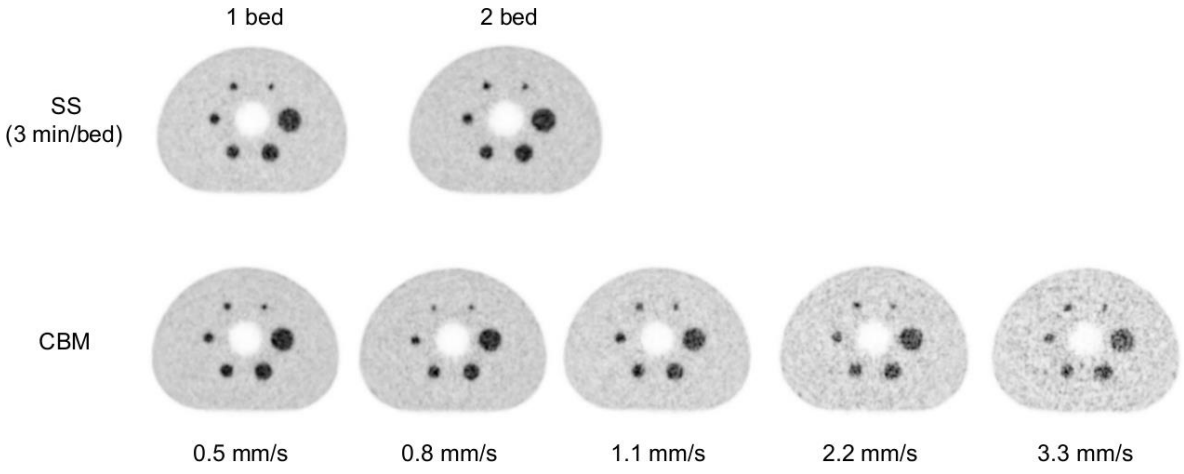

FIGURE 5. The visibility of the hot spheres. The visual score of the 10-mm sphere is not different between the SS 2-bed acquisition and 0.8 mm/s of the CBM method. In the CBM method, the visual score decreased as the bed speed increased.

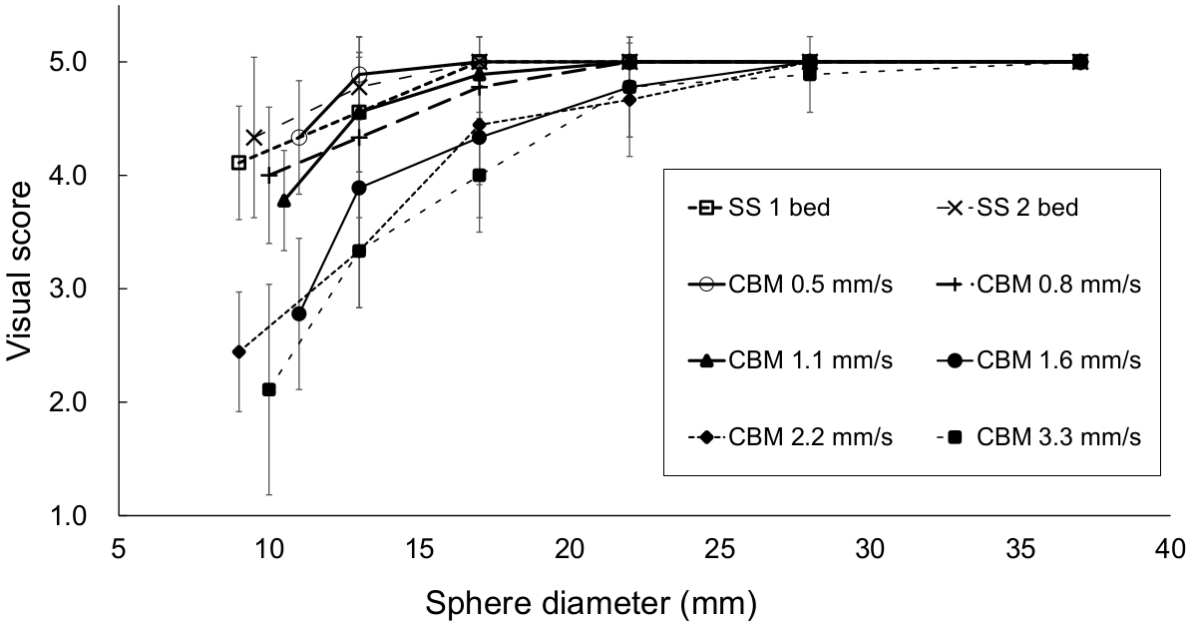

FIGURE 6. The $NEC_{phantom}$ of the SS and CBM methods. In the CBM method, the $NEC_{phantom}$ significantly decreased as the bed speed increased. Bed speeds of 1.1 mm/s or faster showed significantly inferior $NEC_{phantom}$ to that in the SS 2-bed method.

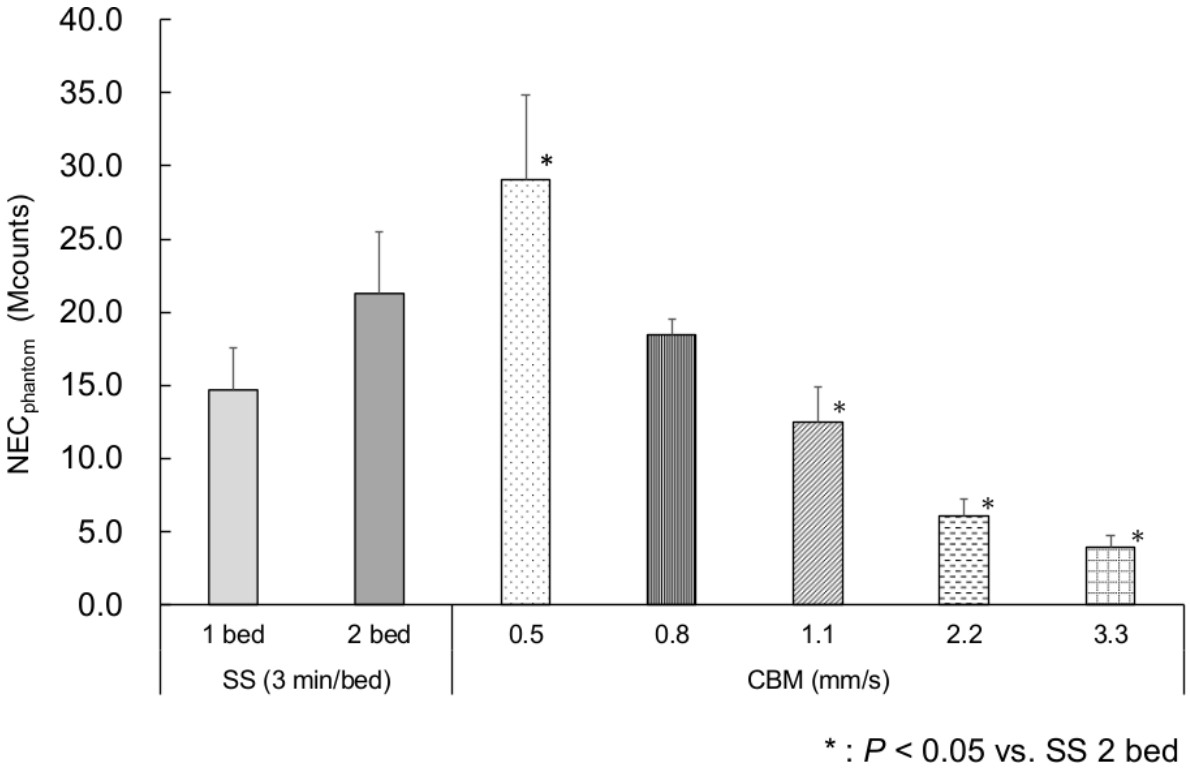

FIGURE 7. The physical assessment of position emission tomography image quality of the SS and CBM methods. (A) $Q_{H,10mm}$ was not significantly different between the SS and CBM methods and among the different bed speeds in the CBM method. (B) Bed speeds of 1.1 mm/s or faster showed significantly inferior N_{10mm} to that in the SS method. (C) The Q_{10mm}/N_{10mm} in the CBM method with bed speeds of 2.2mm/s or faster was significantly lower than that in the SS 2-bed method.

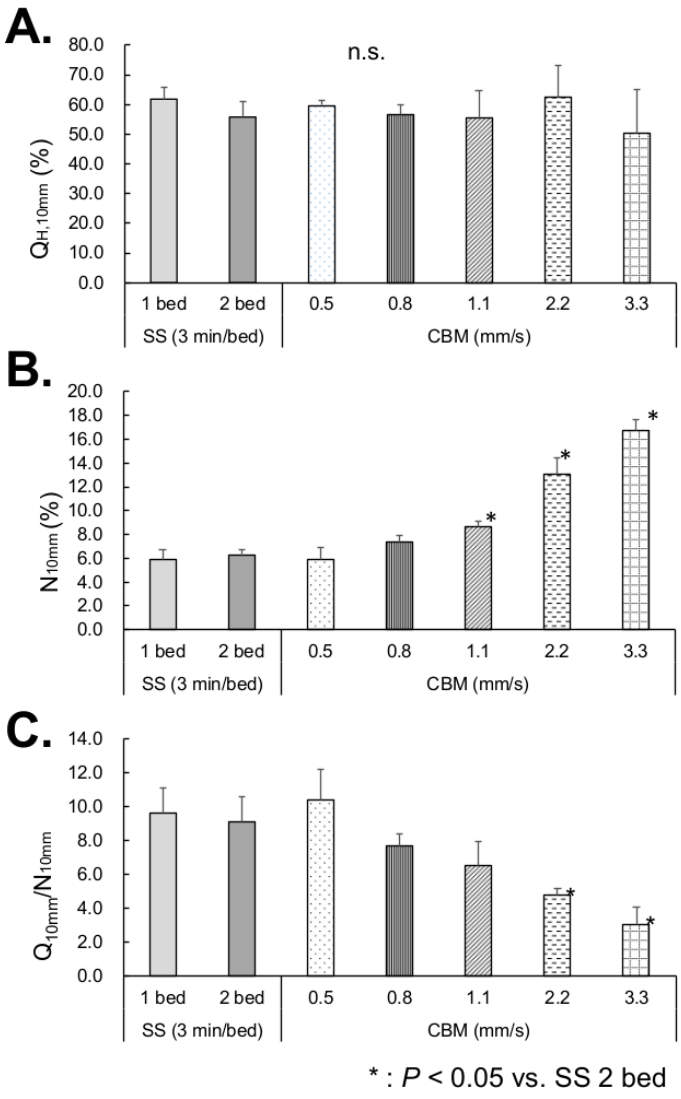

Graphical Abstract

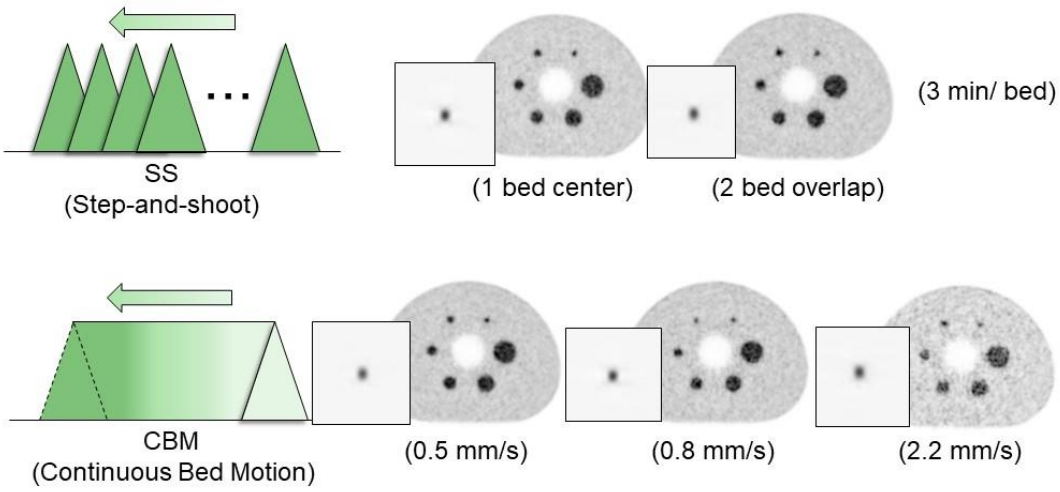

Supplemental Figure 1. NEMA IEC Body phantom. (A) A blueprint of the body phantom, (B) A photograph of the body phantom.